Non-steady-state Stomatal Conductance Modeling and Its Implications: From Leaf to Ecosystem

Ke Liu[1], Yujie Wang[1], Troy Magney[2], and Christian Frankenberg[1,3]

[1]Division of Geological and Planetary Sciences, California Institute of Technology, Pasadena, California 91125, USA
[2]Department of Plant Sciences, University of California, Davis, CA 95616, USA
[3]Jet Propulsion Laboratory, California Institute of Technology, Pasadena, California 91109, USA

Correspondence: Ke Liu (klliu@caltech.edu) and Christian Frankenberg (cfranken@caltech.edu)

Abstract. Accurate and efficient modeling of stomatal conductance (g_s) has been a key challenge in vegetation models across scales. Current practice of most land surface models (LSMs) assumes steady-state g_s and predicts stomatal responses to environmental cues as immediate jumps between stationary regimes. However, the response of stomata can be orders of magnitude slower than that of photosynthesis, and often cannot reach a steady state before the next model time-step, even on half-hourly time scales. Here, we implemented a simple dynamic g_s model in the vegetation module of an LSM developed within the Climate Modeling Alliance, and investigated the potential biases caused by the steady state assumption from leaf to canopy scales. In comparison with steady-state models, the dynamic model better predicted the coupled temporal response of photosynthesis and stomatal conductance to changes in light intensity using leaf measurements. In ecosystem flux simulations, while the impact of g_s hysteresis response may not be substantial in terms of daily or monthly integrated canopy fluxes, our results suggested the importance of considering this effect when quantifying fluxes in the mornings and evenings, and interpreting diurnal hysteresis patterns observed in ecosystem fluxes. Furthermore, prognostic modeling can bypass the A-C$_i$ iterations required for steady-state simulations and can be robustly run with comparable computational costs. Overall, our study highlights the implications of dynamic g_s modeling in improving the accuracy and efficiency of LSMs, and for advancing our understanding of plant-environment interactions.

1 Introduction

Modeling stomatal conductance (g_s), the opening and closure of tiny pores on leaves, is one of the key elements and challenges in land surface models (LSMs). Stomata regulate the gas exchange rates of plants, allowing the uptake of CO_2 for photosynthetic assimilation while constraining water loss through transpiration (Berry et al., 2010; Damour et al., 2010). The behavior of stomata, especially their responses to environmental variations, plays a significant role in determining the fluxes of carbon, water, and energy between vegetated surfaces and the atmosphere (Berry et al., 2010; Buckley, 2017). Therefore, accurate and efficient modeling of g_s is important for understanding the current Earth system and projecting future changes.

Stomatal conductance has been traditionally predicted with empirical models, relating g_s to photosynthesis rate and environmental cues with estimated parameters from statistical regressions (Ball et al., 1987; Leuning, 1990, 1995; Medlyn et al., 2011; Damour et al., 2010). More recently, efforts have been made to constrain stomatal behavior from the principle of optimizing

25 water use efficiency, i.e., the trade-offs between the carbon gain and water loss of stomatal opening (Wolf et al., 2016; Venturas et al., 2018; Wang et al., 2020). Additional understanding of stomatal response includes plant hydraulic models that consider the transport of water from soil through plants into the atmosphere (soil-plant-atmosphere continuum, SPAC) (Sperry et al., 1998, 2002; Bonan et al., 2014). However, most existing stomatal models, especially those currently used to scale from leaf to canopy level and implemented in LSMs, assume steady states (Vialet-Chabrand et al., 2017). They predict the opening and
30 closure of stomata in stationary regimes, modeling stomatal response to environmental variations as immediate jumps between states (Vialet-Chabrand et al., 2013).

While steady-state models assume that stomatal conductance changes instantaneously with the environment, the temporal response of stomata in reality can often be an order of magnitude slower than the biochemical response of photosynthesis (Pearcy and Seemann, 1990; Vialet-Chabrand et al., 2013), and a steady state is often not reached before the next change in
35 conditions (Lawson and Blatt, 2014; Vialet-Chabrand et al., 2017). This slower response of g_s could further impose regulations on assimilation rate via its effects on intercellular CO_2 concentration (C_i), notably under rapidly-changing incident radiation in natural environments (Kaiser and Kappen, 2000; Vialet-Chabrand et al., 2017). The mismatch and interaction of photosynthesis and stomatal response could lead to temporal variations in water use efficiency (WUE) as well (Lawson et al., 2011; Venturas et al., 2018). These can all lead to biases and it is important to consider non-steady-state temporal responses of g_s for more
40 accurate predictions of ecosystem fluxes. Additionally, the inclusion of this factor may also contribute to the hysteresis of plant responses and ecosystem fluxes observed in natural diurnal cycles (Vialet-Chabrand et al., 2013), e.g. evapotranspiration (ET) rates tend to be higher in the afternoon under the same incoming radiation, while canopy conductance overall decreases. These patterns have often been attributed solely to the asymmetry of meteorological variables, especially in temperature and vapor pressure deficit (Zeppel et al., 2004; Bai et al., 2015; Gimenez et al., 2019; Oogathoo et al., 2020; Lin et al., 2019).

45 The current practice of employing g_s models that assume steady-states requires iterations to converge to stable solutions at each simulation step. At the leaf level, this typically involves two nested iteration loops, first to solve the coupled photosynthesis-stomatal conductance model for C_i, and then to solve the leaf energy budget for leaf temperature (Collatz et al., 1991; Bonan et al., 2018), as g_s affects latent heat flux through transpiration. This approach can potentially lead to numerical issues (Sun et al., 2012) and increased computational costs, particularly when upscaling with complex canopies, where angular distribution
50 setups are necessary (Wang and Frankenberg, 2022). However, by utilizing prognostic updates of variables, a dynamic model could simplify simulation steps and improve computational efficiency, enabling runs at finer temporal resolutions.

Moreover, accurate parameter estimation with steady-state models (e.g. linear fitting for the slope g_1 in empirical models) necessitates measurements to be taken after reaching each equilibrium (Leuning, 1990; Miner et al., 2017). Depending on wide-ranging stomatal response speeds (McAusland et al., 2016), obtaining one accurate response curve could take several hours
55 (Liozon et al., 2000; Duarte et al., 2016). Too short of a time step could result in overestimation, underestimation, or unstable results of parameter estimates with steady-state assumptions (Xu and Baldocchi, 2003), which may often be overlooked (Miner et al., 2017). Alternatively, estimates can be approached with a prognostic model by fitting the entire response curve, where steady-state measurements are not fundamentally necessary.

Limitations of steady-state stomatal modeling have driven efforts to develop dynamic models, primarily at the leaf level
(Damour et al., 2010; Vialet-Chabrand et al., 2017). Based on observed variations of g_s, analytical equations of sigmoidal or
exponential response have been commonly used (Naumburg and Ellsworth, 2000; Noe and Giersch, 2004; Vialet-Chabrand
et al., 2013; Vialet-Chabrand et al., 2017; Martins et al., 2016; McAusland et al., 2016); directly adding time-dependent terms
into traditional steady-state models has also been proposed (Matthews et al., 2018). While these models have demonstrated
effective performance in reproducing leaf-level responses to light intensity in controlled conditions, the impacts of including
temporal stomatal dynamics on the simulations of larger-scale fluxes under coupled variations in the natural environment
(e.g., transpiration in the coupled diurnal cycles of radiation, temperature, and vapor pressure deficit (VPD)) have not been
investigated. This may be partly due to the parametrization and complexity of many models optimized for leaf-scale predictions
(Kirschbaum et al., 1988; Vialet-Chabrand et al., 2016), which constrains the feasibility of scaling them to the canopy level in
LSMs.

In this study, we aim to: 1) implement a simplified dynamic stomatal model in the CliMA-Land model, i.e., the land component of a new generation Earth system model within the Climate Modeling Alliance (CliMA); 2) test model performance on
leaf-level measurements and demonstrate an alternative method of parameter estimation with the non-steady-state model in a
Bayesian nonlinear inversion framework; 3) compare simulations of the dynamic model with traditional steady-state modeling,
primarily focusing on the differences in predictions of canopy fluxes and responses to coupled environmental variations on
different time scales.

2 Methods and Materials

2.1 Model framework

2.1.1 Dynamic stomatal modeling

The current steady-state modeling approach in LSMs requires convergence of nested iteration loops to solve leaf fluxes at each
time step (Figure 1a) (Bonan et al., 2018). In this study, we proposed to replace the inner loop for steady solutions of the
coupled photosynthesis-stomatal conductance ($A_n - g_s$) model with prognostic updates of g_{sw} at finer time steps (Figure 1b).

At each step, instead of assuming a initial C_i and iterating until convergence, our framework starts with an initial g_{sw} (e.g.
for the first time step of a diurnal simulation from midnight, this can be set as the minimal conductance in dark). Then solves
A_n and C_i with biochemical demand and diffusive supply of internal CO_2 (Figure 1). For instance, when applying the Farquhar
photosynthesis model for C3 plants (Farquhar et al., 1980), with a given g_{sw}, the RubisCO limited rate (A_c) and light limited
rate A_j are calculated using:

$$A_c = V_{cmax} \cdot \frac{C_i - \Gamma^*}{C_i + K_m} = g_{lc} \cdot (C_a - C_i) + R_d, \tag{1}$$

$$A_j = J \cdot \frac{C_i - \Gamma^*}{4C_i + 8\Gamma^*} = g_{lc} \cdot (C_a - C_i) + R_d. \tag{2}$$

where the middle parts in Eq. 1 and Eq. 2 represent the biochemical demand, and the right part represents the diffusive supply limitation of photosynthesis. V_{cmax} is the maximum carboxylation rate, C_{a} is the ambient CO_2 concentration, R_{d} is the respiration rate, Γ^* is the CO_2 compensation point with the absence of respiration, J is the electron transport rate, K_{m} is the Michaelis-Menten's coefficient, g_{lc} is the leaf total conductance to CO_2, which can be calculated using: $g_{\mathrm{lc}}^{-1} = g_{\mathrm{bc}}^{-1} + 1.6 g_{\mathrm{sw}}^{-1} + g_{\mathrm{m}}^{-1}$, with g_{bc} the boundary conductance to CO_2 and g_{m} the mesophyll conductance. Note that computing A_{c} or A_{j} requires solving for C_{i} first. With a known g_{lc} from g_{sw} at each time-step, rearranging Eq. 1 and Eq. 2 allows for the analytical solution of C_{i}, A_{c} and A_{j}, respectively.

For prognostic updates of g_{sw}, we implemented a simplified dynamic model, adapted from previous studies on leaf-level prognostic modeling (Kirschbaum et al., 1988; Rayment et al., 2000; Noe and Giersch, 2004; Vialet-Chabrand et al., 2016):

$$\frac{\Delta g_t}{\Delta t} = \frac{(g_{\mathrm{ss}} - g_t)}{\tau} \tag{3}$$

where Δt is the time step of the simulation, g_t represents the conductance at the current time step, g_{ss} is the target conductance calculated with steady-state models at the current conditions, and τ is the time constant, representing the time scale of stomatal responses.

As indicated in the flow chart (Figure 1), our dynamic modeling avoids nested iterations for steady solutions while requires updates of variables at finer time steps (e.g. 5-10 min, compared to 30 or 60 min time steps of current LSMs) for the stability of simulations, which we tested and discussed in Section 2.3.3 and 3.3. The prognostic updates of leaf temperature can be implemented accordingly, but as it is not within the scope of this study, we prescribed the leaf temperature updates with measurements in our simulations.

2.1.2 Implementation in LSM

CliMA Land (https://github.com/CliMA/Land), a new generation LSM, is highly modularized and offers flexible model schemes (Wang et al., 2021, 2023), enabling easy implementation and assessment of the dynamic stomatal model across scales. In this study, we used the classic photosynthesis model developed by Farquhar et al. (1980) for C3 plants. For stomatal conductance, we implemented the non-steady-state modeling framework in CliMA Land, and the steady-state g_{s} responses were predicted using the Ball-Berry model (Ball et al., 1987) and the Medlyn model (Medlyn et al., 2011).

2.2 Performance on leaf level measurements

2.2.1 Leaf gas exchange

To test our model and determine key parameters, we recorded light response curves of grape (*Vitis vinifera*) and walnut (*Juglans regia cv.*) leaves using a LI-6800 portable photosynthesis system (LI-COR, Inc., Lincoln, NE, USA). Saplings of *Vitis vinifera* and *Juglans regia cv.* were planted in 5-gallon pots with UC soil mix. 44.4 mL of Osmocote® Smart-Release® Plant Food Plus fertilizer were added to each pot. The plants were grown in a UC Davis lath house. The plants were watered to maintain around 75 percent of completely saturated soil by weight (details in Meeker et al. (2021)). The youngest, fully expanded, intact
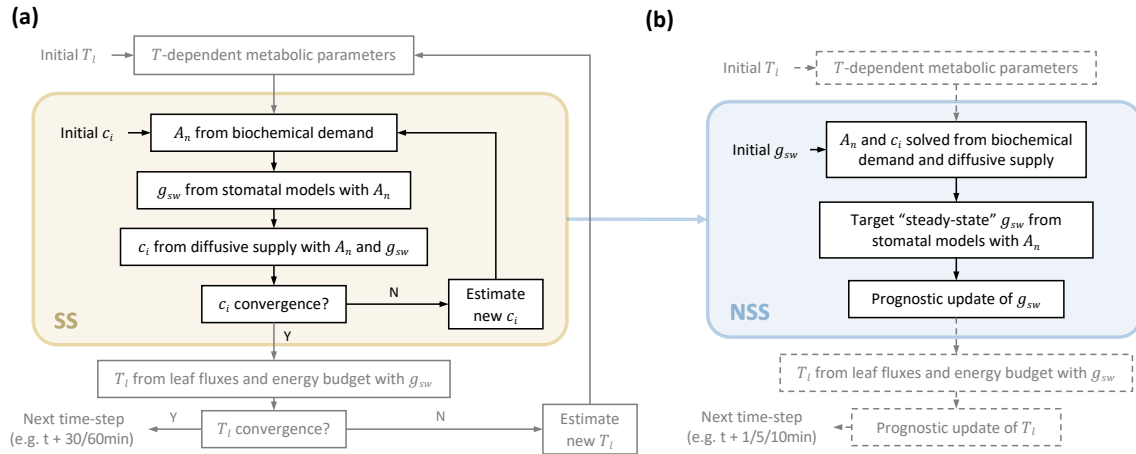
Figure 1. Comparison of leaf flux calculation flows in (a) steady-state (SS) and (b) non-steady-state (NSS) dynamic modeling. (a) illustrates the two nested loops at each time step in the current practice of steady-state framework, adapted from Bonan et al. (2018). The inner iteration in the light yellow box represents the flow of solving the coupled photosynthesis-stomatal conductance (A_n-g_s) model for C_i. The outer solves the leaf energy budget for leaf temperature (T_l). The focus of this study is to implement and compare a dynamic modeling framework to the A_n-g_s model, illustrated in light blue box in (b), where, instead of iterating for steady solutions, g_{sw} is updated prognostically at finer time steps, based on environmental conditions and a simplified dynamic model (Section 2.1.1). This NSS framework of modeling g_{sw} also allows prognostic updates of T_l. As its implementation is not within the scope of this study, related flows are shown in dashed parts.

120 leaf was chosen and dark-adapted for 30 min. During the measurements, the photosynthetic photon flux density (PPFD) was sequentially increased following the gradient of 50, 100, 200, 400, 600, 900, 1200, 1500, 1800 μmol m^{-2} s^{-1}, with a time step of 30 min at each light level. The chamber air temperature was set at 25 °C; CO2 partial pressure was controlled at 400 ppm; the relative humidity in the chamber was maintained around 50%.

2.2.2 Parameter optimization

125 We applied a Bayesian nonlinear inversion framework (Rodgers, 2000; Dutta et al., 2019) to jointly fit the response curves of the net photosynthetic assimilation (A_n) and stomatal conductance (g_s) for each leaf with the non-steady-state model. The forward problem in this case can be represented as follows:

$$y = \mathcal{F}(X; b) + \epsilon; \tag{4}$$

where y represent the measurements, i.e. the light response curves of both A_n and g_s (see Section 2.2.1); $\mathcal{F}$ represents the
130 forward model, CliMA-Land with the dynamic g_s model (see Section 2.1); X is the state vector of parameters to be retrieved, which in our case includes: the maximum carboxylation rate (V_{cmax}), the slope (g_1) and the minimum conductance (g_0) of the BB model, the mesophlly conductance (g_m) (Sun et al., 2014), and the time constant (τ). We also included a scaling factor for A_n, to account for variations in the respiration rate and the ratios between CO_2 and H_2O fluxes; b is the vector of other

parameters that have influences the measurements, are known to some accuracy but not intended to be retrieved, e.g. the ratio

between J_{max} (the maximum electron transport rate) and V_{cmax}, which is assumed to be 1.6 in this study but may vary across conditions (Medlyn et al., 2002); and ϵ is the error term.

The Levenberg–Marquardt (LM) iterations (Levenberg, 1944; Marquardt, 1963; Rodgers, 2000) were utilized to solve the nonlinear inversion problem and find the best estimate of key parameters:

$$x_{i+1} = x_i + \left((1+\gamma)S_a^{-1} + K_i^T S_\epsilon^{-1} K_i\right)^{-1} \left(K_i^T S_\epsilon^{-1}[y - F(X_i)] - S_a^{-1}[x_i - x_a]\right) \tag{5}$$

where x_a is the prior estimate of the state (in this study, V_{cmax}: 70 mol m^{-2}s^{-1}, g_1: 9, g_0: 0.03 mol H$_2$O m^{-2} s^{-1}, g_m: 0.4 mol CO$_2$ m^{-2} s^{-1}, τ: 600 s, $scaling_A$: 1); S_a is the prior covariance matrix, assumed to be purely diagonal, with Gaussian uncertainties in the prior state (the assumed prior standard deviation of V_{cmax}: 30, g_1: 3, g_0: 0.005, g_m: 0.02, τ: 100, $scaling_A$, 0.01). K_i is the Jacobian matrix at the ith iteration. γ is adjusted at each step, ensuring that each update of the state vector moves towards minimizing the cost function. S_ϵ is the error covariance matrix; in our case, errors were assumed to be mainly from measurement uncertainties and calculated based on the standard deviation and mean of the ΔCO$_2$ and ΔH$_2$O in LI-6800 measurements.

2.2.3 Uncertainties in traditional parameter estimation

To illustrate the influence of time steps on parameter estimation in the traditional method, which assumes steady states, we used the NSS model to generate leaf response curves to the same PPFD sequence but with different time intervals. For example, in the 5-min time step simulation, light intensity input jumped every 5 minutes, and measurements were assumed to be taken right before the next jump, following the traditional method. We then employed these curves to calculate the estimated g_1 and g_0 values using the traditional linear fitting method for the Ball-Berry model. The potential biases were assessed by comparing fitted parameters with different applied time steps.

2.3 Comparison of models in diurnal cycles

To compare the prediction of surface flux from models with different assumptions and to assess the potential bias of steady-state modeling, we employed high temporal resolution radiation measurements in the field as inputs and ran CliMA Land with both setups. We evaluated and compared the simulation results on both the leaf and canopy flux scales.

2.3.1 Diurnal variations of radiations

Photosynthetically active radiation (PAR) in a crop field (42.481677°N, 93.523521°W) was recorded with a LI-190R quantum sensor (LI-COR, Inc., Lincoln, NE, USA) at 1 s temporal resolution during August 2017.

In addition to the fluctuations of total incoming photon density that the PAR sensor can provide, canopies in natural environments also experience variations in the fraction of direct and diffuse components in the total radiation. This variation affects the distribution of PAR received by individual leaves across different layers of the canopy structure (Durand et al., 2021). To account for this effect, we employed an empirical fitting with the hourly radiation data from ERA5 (Figure 2), to estimate the
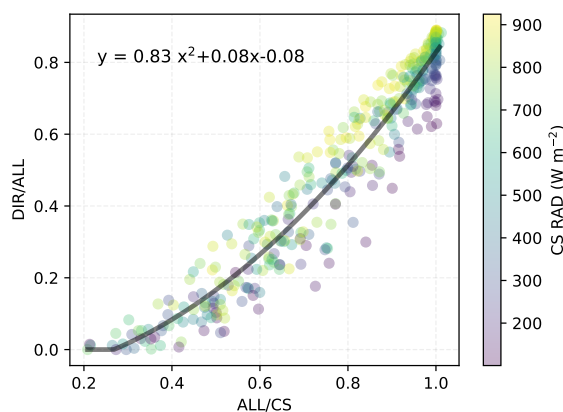
Figure 2. The empirical relationship between the direct radiation (DIR) fraction and the ratio between the total downward solar radiation (ALL) and the clear sky radiation (CS) in August 2017, filtered by 100 W m^{-2} CS radiation. Radiations are from the ERA5-Land hourly dataset.

165 partitioning between the direct and diffuse radiation (Boland et al., 2001). The empirical relationship was then applied to high temporal resolution PAR measurements to obtain the direct and diffuse components in the recorded total radiation, which were used as inputs for simulations at the canopy scale.

2.3.2 Environmental drivers and plant traits

Meteorological variables (e.g. air temperature, dew-point temperature, volumetric soil water, wind speed etc.) from the ERA5-
170 Land hourly dataset were input as environmental drivers for the simulations on the canopy scale. Linear interpolations were applied for runs at sub-hourly time steps. Key plant traits (e.g. V_{cmax}, g_1, leaf area index (LAI)) were extracted from several globally gridded datasets using GriddingMachine (Wang et al. 2022; Croft et al. 2020; Butler et al. 2017; Luo et al. 2021; De Kauwe et al. 2015; Yuan et al. 2011; He et al. 2012, ; also see Wang et al. (2023) for detailed information on global scale datasets used in CliMA-Land).

175 ### 2.3.3 Model simulations

In the comparison of the dynamic (non-steady-state, NSS) and steady-state (SS) modeling, a time constant of 900 s was used for the prognostic model, based on the average time constant retrieved from leaf response curve in Section 2.2.1 and 2.2.2 as well as previous studies on the time constant variations (Vialet-Chabrand et al., 2013; McAusland et al., 2016; Vialet-Chabrand et al., 2017). In the SS runs, iterations were employed to converge to steady-state solutions at each time step.

180 For the leaf-scale runs, we used the key parameters retrieved in previous sections and tested model predictions for an ideal clear-sky day. To investigate the differences in ecosystem fluxes, we ran and assessed the NSS and SS simulations using a time step of 1 minute, with the inputs of meteorological drivers and plant traits at the location of the PAR measurement for

the month of August 2017. In order to further evaluate the potential contribution of g_s hysteresis to the observed diurnal hysteresis of ecosystem fluxes, we compared the standard runs with the model predictions where environmental variables (e.g.

185   temperature, VPD, soil water content (SWC), etc.) were held constant over the daytime (as the mean of daytime values in each day). This approach allowed us to isolate the effect of hysteresis in g_s response and assess its potential contribution to the observed diurnal hysteresis of canopy and ecosystem fluxes.

Furthermore, to test the stability of prognostic modeling and assess the computational cost, we compared NSS simulations using different time steps, as well as the SS simulation run at a time step of 30 min, which is commonly used in current LSMs.

190   This enabled us to evaluate the sensitivity of NSS predictions to the time step used, as well as compare the computational cost for stable NSS runs and standard SS simulations. We resampled the environmental drivers from ERA5 and the PAR sensor to match the temporal resolution of the simulations, while maintaining constant average values for each diurnal cycle across simulations with different time steps.

3   Results

195   ### 3.1   Model performance and parameter estimates on leaf measurements

With the parameters estimated from the LM inversion framework, the non-steady-state model well predicted the temporal responses of g_{sw} and A_n (Figure 3). The model was able to capture the gradual increases of g_{sw} and A_n after each step change in $APAR$, and the reproduced curves were close to the measurements, with all R^2 higher than 0.98. Fitted time constant τ showed a variation across leaves (292 s and 2028 s for the *Vitis vinifera* leaf and the *Juglans regia cv.* leaf, respectively).

200   The relative difference in the time constant matched with the variations of response speed observed in the measured response curves (Figure 3). Compared to the SS model, the dynamic model provided more accurate prediction to the temporal responses. The improvements in R^2 were more prominent in the predictions of the *Juglans regia cv.* leaf responses, which have a larger time constant, than in those of the *Vitis vinifera* leaf. Other parameters estimated for the *Vitis vinifera* leaf include V_{cmax}, 71 mol m^{-2}s^{-1}, g_1, 11.3, g_0, 0.023 mol H$_2$O m^{-2} s^{-1}, g_m, 0.18 mol CO$_2$ m^{-2} s^{-1}, $scaling_A$, 1.1; for the *Juglans regia cv.* leaf,

205   V_{cmax}, 152 mol m^{-2}s^{-1}, g_1, 3.9, g_0, 0.052 mol H$_2$O m^{-2} s^{-1}, g_m, 0.34 mol CO$_2$ m^{-2} s^{-1}, $scaling_A$, 1.0.

The dynamic model was also able to better capture the temporal variations of internal CO$_2$ concentration (Figure 4). Particularly, the NSS model reproduced the undershooting of the intercellular CO$_2$ concentration (C_i) after each step change in light intensity, which resulted from the differences in the speed of g_s and A_n responses and their interactions. As shown in the measured time series (Figure 3), after each increase in the incident light, photosynthesis was able to respond almost instanta-

210   neously, leading to a rapid decrease in C_i, while stomata opened gradually, slowly bringing up C_i over time. This then led to a gradual rise of A_n after the initial rapid response, indicating the regulation of g_s on A_n through its impacts on the internal CO$_2$ supply. In the meantime, the increasing A_n further promoted the opening of stomata with a higher internal CO$_2$ demand, demonstrating their coupled responses to environmental variations.

With the dynamic model and optimized parameters that accurately reproduced the measured leaf responses, we investigated

215   the influence of time steps used in light response curves (i.e. the length of intervals between step changes in light intensity) on
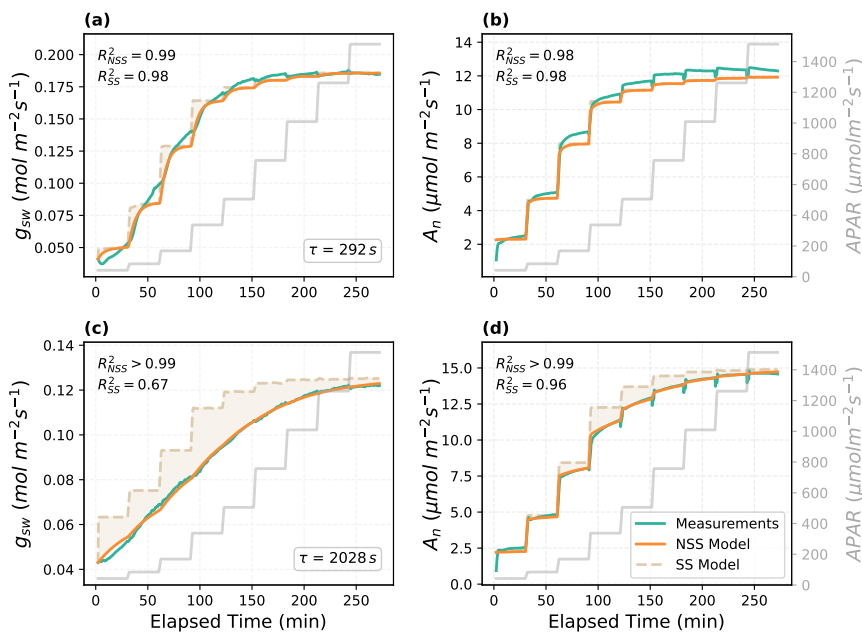
Figure 3. Modeled and measured temporal responses of the stomatal conductance (g_{sw}) and net photosynthesis rate (A_n) to the step changes in APAR for different leaves. The shaded area indicates the difference between the prediction of the steady-state (SS) model and the non-steady-state (NSS) dynamic model. (a-b) The temporal responses of the *Vitis vinifera* leaf, (c-d) the *Juglans regia cv.* leaf.
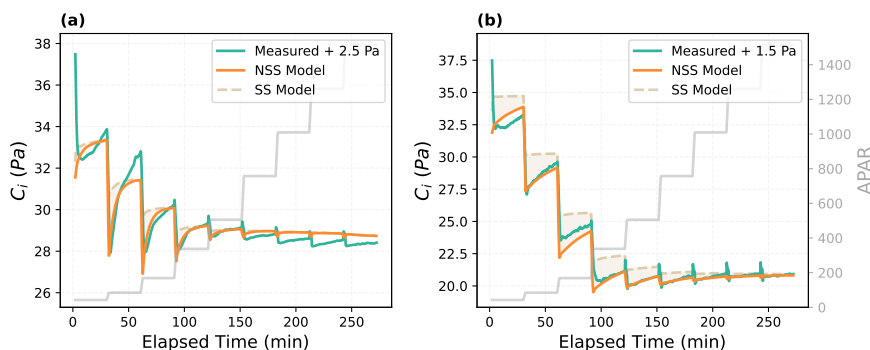

Figure 4. Modeled and measured temporal responses of intercelluar CO_2 concentration (C_i) for (a) the *Vitis vinifera* leaf and (b) the *Juglans regia cv.* leaf. As indicated in labels, measured curves were shifted to illustrate the comparison of modelled and measured response patterns, as the absolute values are not directly comparable due to different assumptions of LI-6800 and CliMA-Land in calculating the internal CO_2. The shaded area indicates the difference between the prediction of the steady-state (SS) model and the non-steady-state (NSS) dynamic model.
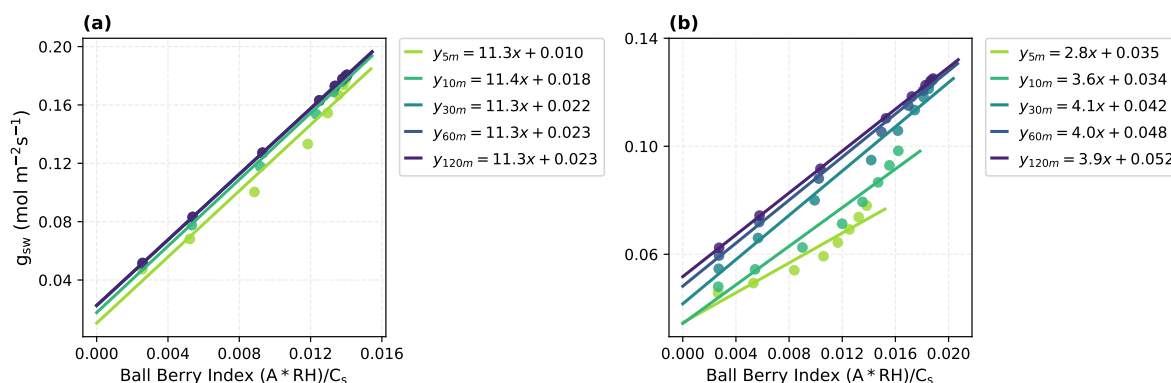
Figure 5. Parameter estimates for the Ball-Berry model with the traditional linear fitting method using model-reproduced response curves with different time steps (5 min, 10 min, 30 min, 60 min, 120 min). (a) fitting results for the *Vitis vinifera* leaf, (b) the *Juglans regia cv.* leaf. Corresponding Ball-Berry index and g_{sw} are plotted, along with the fitted lines and parameters (i.e. the Ball-Berry slope, g_1, and the intercept, namely, the minimum conductance, g_0).

parameter estimates obtained with traditional methods (Figure 5). The results showed that, particularly for the *Juglans regia cv.* leaf that has a long time constant over 2000 s, the values and relationship between the Ball-Berry index and g_{sw} varied significantly depending on the time step used, resulting in notable uncertainties in fitted g_1 and g_0 with too short of a interval to reach equilibrium. This also suggested that obtaining reliable estimates for this leaf using the traditional method could require more than an hour for stable readings at each step.

3.2 Model comparison in diurnal cycles

3.2.1 Leaf responses

To compare NSS and SS models over the course of a day, we evaluated the differences in their predictions of leaf responses to an ideal diurnal cycle of light with other environmental conditions (e.g. temperature, VPD, CO_2) held constant (Figure 6). Results showed that compared to NSS, the SS model predicted a higher A_n and g_s in the morning, as it assumed the stomata could respond immediately to an increase in light, whilst in the more realistic NSS simulation, the gradual opening of stomata limited the CO_2 supply for photosynthesis with a lower C_i. The opposite was true for the afternoon, but the overestimation of A_n and g_s in SS modeling in the morning was more significant than the underestimation in the afternoon, leading to slightly higher diurnally-integrated predictions than those of the NSS model. This was due to the fact that in the course of sunset, the major limiting factor on productivity was the decreasing light, in contrast to the sunrise where it was the available C_i regulated by g_s responses that mainly constrained A_n increases. The relative differences (RDs) in integrated g_s in the morning and afternoon were both higher than those of the photosynthesis, reflecting the differences in the response speed.
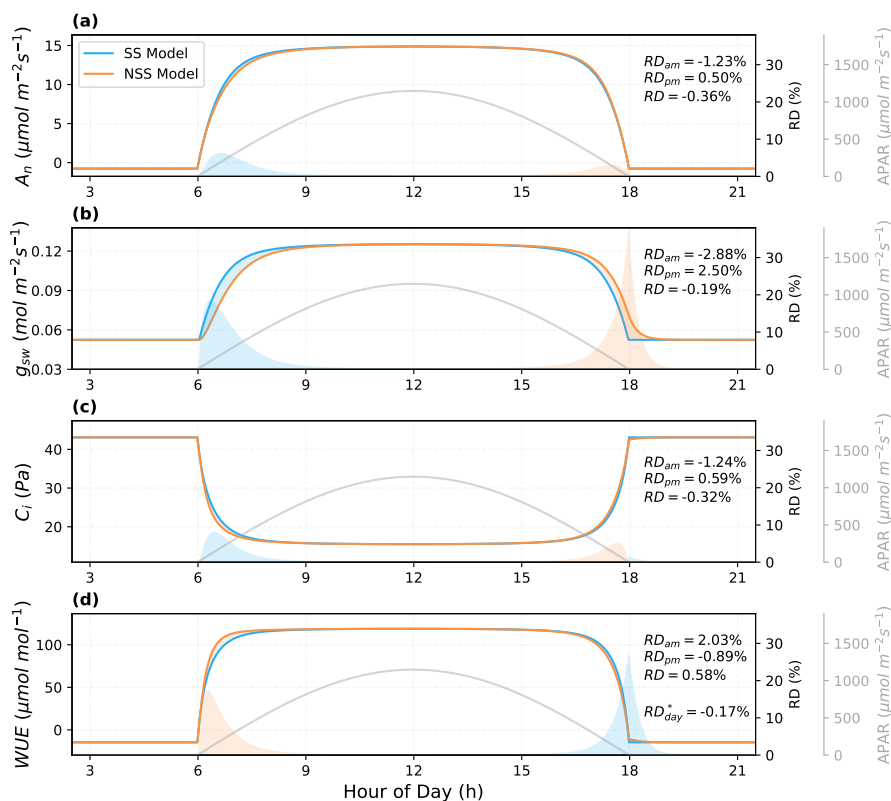
Figure 6. Predictions of the leaf diurnal course of (a) net photosynthesis rate (A_n), (b) stomatal conductance to water vapor (g_{sw}), (c) intercellular CO_2 concentration (C_i), and (d) intrinsic water-use efficiency (WUE) for a leaf with a stomatal time constant of 900 s in an ideal clear-sky day. Other environmental conditions (e.g. leaf temperature, VPD) were held constant. The shaded areas indicate the differences between the NSS and SS simulations (blue: SS > NSS; orange: SS < NSS), both in absolute and relative terms. Relative differences (RD, NSS - SS) in the temporal integrals are also presented, for morning (am, 5:00-12:00), afternoon (pm, 12:00-19:00), and daytime (5:00-19:00). RD^* of WUE represents the ratio between integrated A_n and g_{sw}, differing from the RD, the integral of the instantaneous WUE during the daytime.

The differences in predictions of A_n and g_{sw} responses also led to RDs in the intrinsic water-use efficiency (WUE, i.e. the ratio between A_n and g_{sw}). Although the mean instantaneous WUE during the daytime was higher in the NSS simulation, diurnal WUE calculated from the integrated A_n and g_{sw} was lower. This was because the gradual opening of stomata during the sunrise limited assimilation in the morning, whereas during the sunset, delayed closure led to unnecessary water loss when carbon gain was constrained by low light.

3.2.2 Canopy fluxes

To quantify the impacts of the inclusion of g_s temporal response, we analyzed the simulated canopy fluxes under natural

240 radiation variations and coupled dynamics of environmental conditions. As shown in the examples of diurnal cycle simulations (Figure 7 and 8), the SS model predicted higher variations in instantaneous fluxes in response to rapid fluctuations in radiation, particularly in transpiration rates.

The differences in fluxes between the NSS and SS predictions were not significant when integrated over monthly periods (e.g. the mean RD of transpiration in August 2017, 0.87 %, and the median, 1.0 %), but are notable in diurnal cycles depending

245 on the radiation and other conditions, especially when considering the sub-diurnal scale (e.g. the maximum RD in transpiration for daytime integrals was 2.74 % and the variation of afternoon RDs ranged from -7.4 % to 6.1 %).

The overall tendency to overestimate productivity with traditional SS models was also observed on the canopy scale, as the regulation of g_s hysteresis on the supply of CO_2 for photosynthesis was not considered (Figure 9b). For example, in Figure 7, when rapid spikes of radiation occurred in the afternoon, the speed of g_s response constrained the increases of photosynthesis

250 in the NSS simulation.

In contrast to the leaf-scale results, when accounting for other co-varying environmental drivers (e.g. temperature, VPD, soil water content), the SS model tended to underestimate canopy transpiration rates, although RDs in the mornings and afternoons varied depending on the radiation dynamics (Figure 7b, Figure 8b, Figure 9a). This could be because the transpiration rates were determined by both g_{sw} and VPD. During the daytime, VPD usually increased following the air temperature and peaked in

255 the afternoon, when the slow response of stomata to the increasing VPD and decreasing radiation could result in excess water loss (Figure 8b, Figure 9 a and c). The overestimation of productivity and underestimation of transpiration in SS simulations also led to further overestimation of the WUE.

3.2.3 Diurnal hysteresis

To investigate the relative contributions of g_s hysteresis and environmental variables to the hysteresis observed in plant be-

260 haviors and ecosystem fluxes, we separated the effects of these two factors by comparing predicted response curves in NSS and SS simulations with and without diurnal environmental variations (e.g. temperature, VPD, soil water content). While the asymmetry of environmental variables in the diurnal cycle could lead to a modeled hysteresis of g_s in response to radiation, where g_s tended to be lower in the afternoon mainly due to higher VPD and temperature, our results (Figure 10) showed that the kinetic lag of g_s could partially offset this effect (Figure 10 b and d), even presenting an opposite tendency at low radiations.

265 Additionally, only the NSS model simulations predicted a hysteresis of canopy transpiration, with or without the consideration of coupled environmental variations (Figure 10 g and h), in which canopy H_2O fluxes tended to be higher in the afternoon.
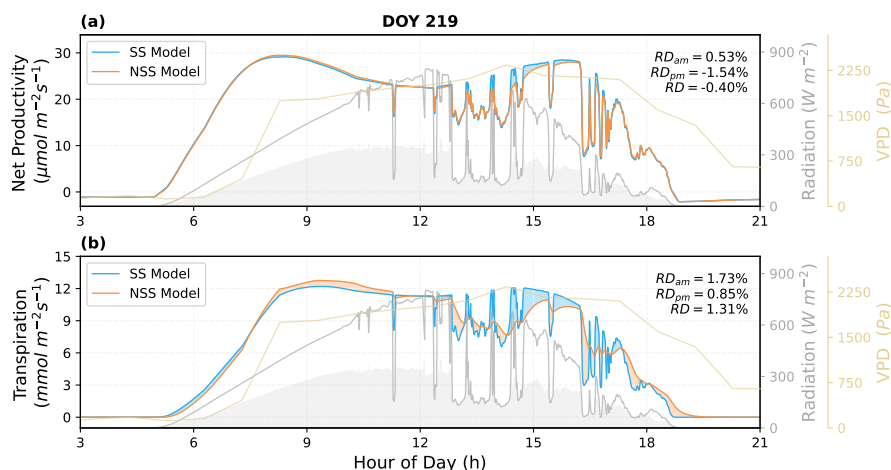
Figure 7. Comparison of the predicted diurnal cycles of ecosystem fluxes, (a) the net productivity and (b) the transpiration rate for DOY 219, 2017. The shaded areas in blue and orange indicate the differences between the NSS and SS predictions (blue: SS > NSS; orange: SS < NSS). The shaded areas in gray under the radiation curves represent the diffuse component of the total radiation. Relative differences (RD, NSS - SS) in the temporal integrated fluxes are also presented, for morning (am, 5:00-12:00), afternoon (pm, 12:00-19:00), and daytime (5:00-19:00).
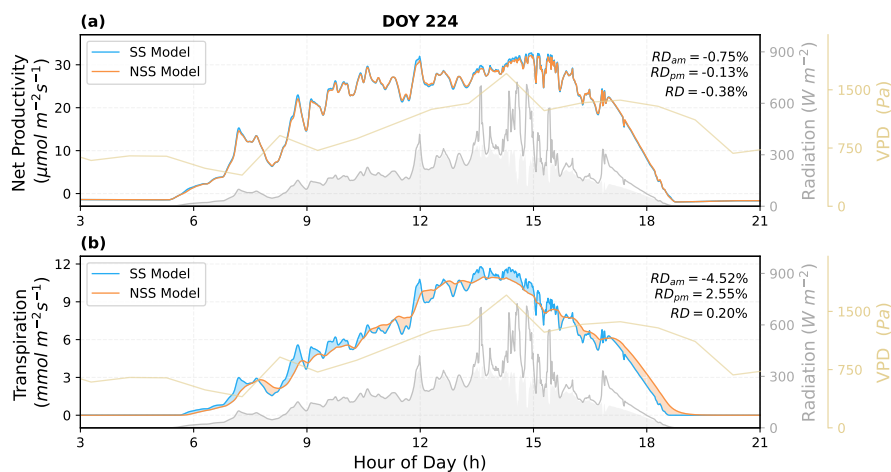

Figure 8. Comparison of the predicted diurnal cycles of ecosystem fluxes, (a) the net productivity and (b) the transpiration rate for DOY 224, 2017. The shaded areas in blue and orange indicate the differences between the NSS and SS predictions (blue: SS > NSS; orange: SS < NSS). The shaded areas in gray under the radiation curves represent the diffuse component of the total radiation. Relative differences (RD, NSS - SS) in the temporal integrated fluxes are also presented, for morning (am, 5:00-12:00), afternoon (pm, 12:00-19:00), and daytime (5:00-19:00).
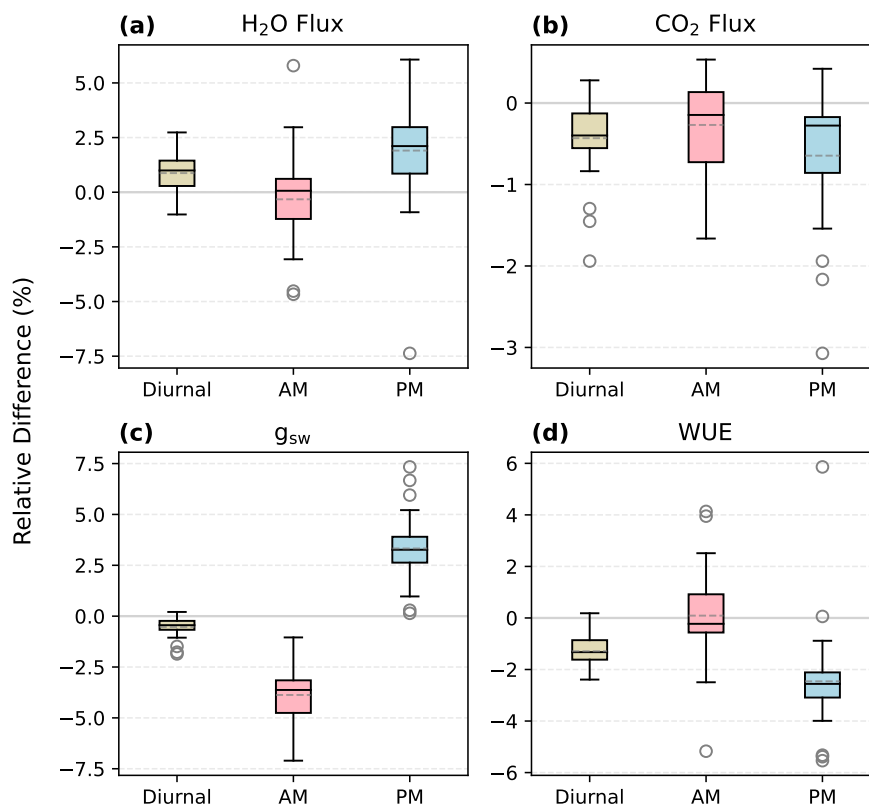
Figure 9. Relative differences (NSS - SS) in the predicted daytime-mean fluxes of the NSS (time step: 1 min) and SS (1 min) simulations for August 2017. The solid line in each box indicates the median, and the dashed line represents the mean. (a) RDs in H_2O flux, the transpiration rate, (b) CO_2 flux, the net productivity, (c) Canopy-averaged stomatal conductance to water (g_{sw}), (d) Water-use efficiency (WUE). Diurnal: 5:00-19:00, AM: 5:00-12:00, PM: 12:00-19:00.

3.3 Stability of the dynamic model

We further assessed the sensitivity of the dynamic modeling to the time step of simulation. Figure 11 shows the NSS model was be able to run at a time step of 10 minutes stably and still demonstrated the impacts of gradual g_s responses, as compared to the traditional practice of SS modeling at a time step of 30 minutes.

4 Discussion

In this study, we demonstrated the feasibility and benefits of implementing a non-steady-state stomatal conductance modeling framework from the leaf to canopy scale, in a new generation LSM, CliMA-Land. Our results suggested that compared to traditional steady-state models, the dynamic model was able to provide more realistic and accurate predictions of leaf temporal

275 responses to the changes in light intensity (Section 3.1). In the meantime, modeling g_s with prognostic updates - similar to how plants control their stomata movements gradually in natural environments - neither increased computational cost nor model complexity, as simulations were simplified with iterations to solve for steady states avoided. Sun et al. (2012) pointed out the default 3-step fix-point iteration in CLM4 (the Community Land Model version 4) does not always converge, leading to uncertainties in flux predictions. In our simulations at the canopy scale (Section 3.3), the dynamic model could be stably run

280 at a temporal resolution that presented comparable efficiency to the current practice of 30-minute resolution SS simulations commonly used in LSMs. This also indicates the dynamic model can enable predictions of canopy flux dynamics at a finer time resolution with higher efficiency and accuracy.

With the non-steady-state model, we were able to apply a Bayesian nonlinear inversion framework to jointly fit the light response curves of both A_n and g_s, and obtain estimates for key parameters (Section 3.1). As suggested in our results (Figure 5)

285 and previous studies (Xu and Baldocchi, 2003; Miner et al., 2017), the time step of light response curves can notably influence the estimated parameters obtained from the traditional linear fitting method for steady-state empirical models. Our framework with the dynamic model can help reduce the time required for accurate parameter estimations, particularly for leaves with long time constants, as equilibrium is not required. Although the retrieval setups presented in this study may not be optimal for estimating V_{cmax}, which is typically derived from A-C_i response curves (Medlyn et al., 2002; Miao et al., 2009; Duarte et al.,

290 2016), a similar framework can be applied to other scenarios for estimation of various parameters, including a A-C_i curve for V_{cmax}.

Furthermore, we evaluated how the inclusion of g_s temporal responses could affect model predictions of leaf and canopy fluxes in diurnal cycles with natural environmental variations (Section 3.2.2). The comparison of NSS and SS simulations indicated that, while the differences in monthly fluxes were not significant, effects of g_s temporal dynamics could be notable

295 in diurnal courses and on sub-diurnal scales depending on the conditions. Overall, slow opening of stomata tended to limit productivity responses to rapid radiation increases, and delayed closure of g_s following decreases in radiation or increases in environmental stress (e.g. increasing VPD), results in unnecessary water loss. Both aspects led to overestimation of canopy WUE in traditional steady-state simulations. Similar effects have been noted in studies on leaf-scale response to PPFD fluctuations (Lawson et al., 2011; Lawson and Blatt, 2014; McAusland et al., 2016). This suggests that the temporal hysteresis of g_s

300 can have impacts on the integrated cost (water loss) and benefit (carbon gain) of stomatal behavior in diurnal cycles, especially in highly fluctuating environments (e.g. understory plants experiencing sunflecks), and it is necessary to include its effects on the optimal trade-off to understand and predict stomatal responses with the optimization theory (Cowan and Farquhar, 1977; Vialet-Chabrand et al., 2017).

In addition, the hysteresis of leaf-level g_s response can contribute to the hysteresis patterns at the ecosystem scale, which

305 have often been solely attributed to the asymmetry of environmental variables during the daytime. For instance, higher evapotranspiration (ET) fluxes and sap velocity (i.e. an indicator of plant transpiration rate) have been observed in the field, with explanation often focused on higher VPD in the afternoon following increased air temperature (Zeppel et al., 2004; Gimenez et al., 2019; Oogathoo et al., 2020; Lin et al., 2019). Our simulations showed that the SS model with diurnal environmental variations was unable to reproduce this hysteresis pattern, while it was captured in NSS runs, indicating the significance of

310 considering g_s temporal dynamics when interpreting diurnal hysteresis in transpiration (Section 3.2.3). Moreover, observed patterns of lower g_s in the afternoon have also been commonly explained with similar environmental asymmetry (Bai et al., 2015; Lin et al., 2019), whilst our results suggested the kinetic lag of g_s could partially offset this effect, and thus should be taken into account in understanding the hysteresis patterns.

Further improvements can be made in applying separate time constants for stomata opening and closing course, as previous
315 studies have suggested different response speeds of increasing and decreasing g_s to a step change in irradiance (McAusland et al., 2016; Vialet-Chabrand et al., 2017; Matthews et al., 2018). More comprehensive measurements of temporal response curves across species and conditions can also contribute to improving our understanding of the variation of time constant towards better predictions of g_s temporal responses.

The dynamic g_s model enables predictions of temporal changes in latent heat flux through transpiration in leaf energy
320 balance, which allows a similar prognostic framework to be employed for the modeling of leaf temperature. Bonan et al. (2018) implemented a non-steady-state framework for leaf temperature modeling, but as steady-state g_s models were employed, iterations for stable solutions were still required. With the dynamic g_s model presented in this study, the traditional nested iteration loops in leaf flux calculations, which can take up to 40 iterations to solve for a single simulation step in CLM4.5 (Bonan et al., 2018), can be replaced by more efficient and accurate prognostic updates of variables with ordinary differential
325 equations (ODEs). Such an approach can also facilitate better couplings of LSMs with other components in Earth system models (ESMs), where ODE systems are commonly used.

5 Conclusions

We implemented a simplified dynamic stomatal conductance model in CliMA-Land, and evaluated its impacts on model simulations across scales. In comparison with the traditional steady-state model, the dynamic model better predicted the coupled
330 temporal responses of A_n, g_s and C_i observed in leaf measurements. We also found uncertainties in parameter estimation for steady-state g_s models with the traditional linear fitting method, when too short of a time step used resulted in unstable estimates. We proposed an alternative approach using a Bayesian nonlinear inversion framework with a dynamic model, which could help reduce the time investment for estimation, particularly for leaves with long time constants. Our results on canopy-scale simulations suggested that, although the effects of temporal g_s responses on ecosystem fluxes may not be significant in
335 terms of monthly integrals, but should be take into account when predicting diurnal courses and quantifying sub-diurnal scale fluxes, as well as explaining the hysteresis patterns observed in diurnal cycles.

We demonstrated that the more realistic prognostic modeling of gradual g_s response simplified the simulation as iteration loops for solving steady-states at each time step were avoided, and the dynamic model can be run at a finer time resolution that presents comparable computational costs to the current practice of steady-state leaf flux calculation. A similar framework can
340 be extended to leaf temperature modeling which will enable prognostic updates of leaf level variables with higher efficiency and accuracy, towards better couplings of LSMs with other components in Earth system models (ESMs).

16

Code and data availability. We coded our model and did the analysis using Julia, and the current version of the CliMA Land model with the implementation of dynamic stomatal conductance framework is available from the project website: https://github.com/CliMA/LandCliMA. Other code and data sets used in the study will be available in the final manuscript.

345 *Author contributions.* CF, KL and YW designed and conceptualized the study. TM provided the leaf gas exchange measurements. YW developed CliMA Land and helped with the implementation of the dynamic model. KL performed the analysis. KL, CF and YW interpreted the results. KL composed the manuscript with contributions from all authors.

Competing interests. The contact author has declared that neither they nor their co-authors have any competing interests.

References

Bai, Y., Zhu, G., Su, Y., Zhang, K., Han, T., Ma, J., Wang, W., Ma, T., and Feng, L.: Hysteresis loops between canopy conductance of grapevines and meteorological variables in an oasis ecosystem, Agricultural and Forest Meteorology, 214-215, 319–327, https://doi.org/10.1016/j.agrformet.2015.08.267, 2015.

Ball, J. T., Woodrow, I. E., and Berry, J. A.: A Model Predicting Stomatal Conductance and its Contribution to the Control of Photosynthesis under Different Environmental Conditions, in: Progress in Photosynthesis Research: Volume 4 Proceedings of the VIIth International Congress on Photosynthesis Providence, Rhode Island, USA, August 10–15, 1986, edited by Biggins, J., pp. 221–224, Springer Netherlands, Dordrecht, https://doi.org/10.1007/978-94-017-0519-6_48, 1987.

Berry, J. A., Beerling, D. J., and Franks, P. J.: Stomata: key players in the earth system, past and present, Current Opinion in Plant Biology, 13, 232–239, https://doi.org/10.1016/j.pbi.2010.04.013, number: 3, 2010.

Boland, J., Scott, L., and Luther, M.: Modelling the diffuse fraction of global solar radiation on a horizontal surface, Environmetrics, 12, 103–116, https://doi.org/10.1002/1099-095X(200103)12:2<103::AID-ENV447>3.0.CO;2-2, _eprint: https://onlinelibrary.wiley.com/doi/pdf/10.1002/1099-095X%28200103%2912%3A2%3C103%3A%3AAID-ENV447%3E3.0.CO%3B2-2, 2001.

Bonan, G. B., Williams, M., Fisher, R. A., and Oleson, K. W.: Modeling stomatal conductance in the earth system: linking leaf water-use efficiency and water transport along the soil–plant–atmosphere continuum, Geoscientific Model Development, 7, 2193–2222, https://doi.org/10.5194/gmd-7-2193-2014, number: 5 Publisher: Copernicus GmbH, 2014.

Bonan, G. B., Patton, E. G., Harman, I. N., Oleson, K. W., Finnigan, J. J., Lu, Y., and Burakowski, E. A.: Modeling canopy-induced turbulence in the Earth system: a unified parameterization of turbulent exchange within plant canopies and the roughness sublayer (CLM-ml v0), Geoscientific Model Development, 11, 1467–1496, https://doi.org/10.5194/gmd-11-1467-2018, number: 4 Publisher: Copernicus GmbH, 2018.

Buckley, T. N.: Modeling Stomatal Conductance, Plant Physiology, 174, 572–582, https://doi.org/10.1104/pp.16.01772, number: 2, 2017.

Butler, E. E., Datta, A., Flores-Moreno, H., Chen, M., Wythers, K. R., Fazayeli, F., Banerjee, A., Atkin, O. K., Kattge, J., Amiaud, B., Blonder, B., Boenisch, G., Bond-Lamberty, B., Brown, K. A., Byun, C., Campetella, G., Cerabolini, B. E. L., Cornelissen, J. H. C., Craine, J. M., Craven, D., de Vries, F. T., Díaz, S., Domingues, T. F., Forey, E., González-Melo, A., Gross, N., Han, W., Hattingh, W. N., Hickler, T., Jansen, S., Kramer, K., Kraft, N. J. B., Kurokawa, H., Laughlin, D. C., Meir, P., Minden, V., Niinemets, Ü., Onoda, Y., Peñuelas, J., Read, Q., Sack, L., Schamp, B., Soudzilovskaia, N. A., Spasojevic, M. J., Sosinski, E., Thornton, P. E., Valladares, F., van Bodegom, P. M., Williams, M., Wirth, C., and Reich, P. B.: Mapping local and global variability in plant trait distributions, Proceedings of the National Academy of Sciences, 114, E10 937–E10 946, https://doi.org/10.1073/pnas.1708984114, publisher: Proceedings of the National Academy of Sciences, 2017.

Collatz, G. J., Ball, J. T., Grivet, C., and Berry, J. A.: Physiological and environmental regulation of stomatal conductance, photosynthesis and transpiration: a model that includes a laminar boundary layer, Agricultural and Forest Meteorology, 54, 107–136, https://doi.org/10.1016/0168-1923(91)90002-8, 1991.

Cowan, I. R. and Farquhar, G. D.: Stomatal function in relation to leaf metabolism and environment, Symposia of the Society for Experimental Biology, 31, 471–505, 1977.

Croft, H., Chen, J. M., Wang, R., Mo, G., Luo, S., Luo, X., He, L., Gonsamo, A., Arabian, J., and Zhang, Y.: The global distribution of leaf chlorophyll content, Remote Sensing of Environment, 236, 111 479, iSBN: 0034-4257 Publisher: Elsevier, 2020.

Damour, G., Simonneau, T., Cochard, H., and Urban, L.: An overview of models of stomatal conductance at the leaf level, Plant, Cell & Environment, 33, 1419–1438, https://doi.org/10.1111/j.1365-3040.2010.02181.x, number: 9 _eprint:
390   https://onlinelibrary.wiley.com/doi/pdf/10.1111/j.1365-3040.2010.02181.x, 2010.

De Kauwe, M. G., Kala, J., Lin, Y.-S., Pitman, A. J., Medlyn, B. E., Duursma, R. A., Abramowitz, G., Wang, Y.-P., and Miralles, D. G.: A test of an optimal stomatal conductance scheme within the CABLE land surface model, Geoscientific Model Development, 8, 431–452, https://doi.org/10.5194/gmd-8-431-2015, publisher: Copernicus GmbH, 2015.

Duarte, A., Katata, G., Hoshika, Y., Hossain, M., Kreuzwieser, J., Arneth, A., and Ruehr, N.: Immediate and potential long-term effects of
395   consecutive heat waves on the photosynthetic performance and water balance in Douglas-fir, Journal of Plant Physiology, 2016.

Durand, M., Murchie, E. H., Lindfors, A. V., Urban, O., Aphalo, P. J., and Robson, T. M.: Diffuse solar radiation and canopy photosynthesis in a changing environment, Agricultural and Forest Meteorology, 311, 108 684, https://doi.org/10.1016/j.agrformet.2021.108684, 2021.

Dutta, D., Schimel, D. S., Sun, Y., van der Tol, C., and Frankenberg, C.: Optimal inverse estimation of ecosystem parameters from observations of carbon and energy fluxes, Biogeosciences, 16, 77–103, https://doi.org/10.5194/bg-16-77-2019, number: 1 Publisher: Copernicus
400   GmbH, 2019.

Farquhar, G. D., von Caemmerer, S., and Berry, J. A.: A biochemical model of photosynthetic CO2 assimilation in leaves of C 3 species, Planta, 149, 78–90, https://doi.org/10.1007/BF00386231, number: 1, 1980.

Gimenez, B. O., Jardine, K. J., Higuchi, N., Negrón-Juárez, R. I., Sampaio-Filho, I. d. J., Cobello, L. O., Fontes, C. G., Dawson, T. E., Varadharajan, C., Christianson, D. S., Spanner, G. C., Araújo, A. C., Warren, J. M., Newman, B. D., Holm, J. A., Koven, C. D., McDowell,
405   N. G., and Chambers, J. Q.: Species-Specific Shifts in Diurnal Sap Velocity Dynamics and Hysteretic Behavior of Ecophysiological Variables During the 2015–2016 El Niño Event in the Amazon Forest, Frontiers in Plant Science, 10, https://www.frontiersin.org/articles/10.3389/fpls.2019.00830, 2019.

He, L., Chen, J. M., Pisek, J., Schaaf, C. B., and Strahler, A. H.: Global clumping index map derived from the MODIS BRDF product, Remote Sensing of Environment, 119, 118–130, https://doi.org/10.1016/j.rse.2011.12.008, 2012.

410 Kaiser, H. and Kappen, L.: In situ observation of stomatal movements and gas exchange of Aegopodium podagraria L. in the understorey, Journal of Experimental Botany, 51, 1741–1749, https://doi.org/10.1093/jexbot/51.351.1741, 2000.

Kirschbaum, M. U. F., Gross, L. J., and Pearcy, R. W.: Observed and modelled stomatal responses to dynamic light environments in the shade plant Alocasia macrorrhiza, Plant, Cell & Environment, 11, 111–121, https://doi.org/10.1111/1365-3040.ep11604898, _eprint: https://onlinelibrary.wiley.com/doi/pdf/10.1111/1365-3040.ep11604898, 1988.

415 Lawson, T. and Blatt, M. R.: Stomatal Size, Speed, and Responsiveness Impact on Photosynthesis and Water Use Efficiency, Plant Physiology, 164, 1556–1570, https://doi.org/10.1104/pp.114.237107, number: 4 Publisher: American Society of Plant Biologists Section: TOPICAL REVIEWS - FOCUS, 2014.

Lawson, T., von Caemmerer, S., and Baroli, I.: Photosynthesis and Stomatal Behaviour, in: Progress in Botany 72, edited by Lüttge, U. E., Beyschlag, W., Büdel, B., and Francis, D., Progress in Botany, pp. 265–304, Springer, Berlin, Heidelberg, https://doi.org/10.1007/978-3-
420   642-13145-5_11, 2011.

Leuning, R.: Modelling Stomatal Behaviour and and Photosynthesis of Eucalyptus grandis, Functional Plant Biology, 17, 159, https://doi.org/10.1071/PP9900159, 1990.

Leuning, R.: A critical appraisal of a combined stomatal-photosynthesis model for C3 plants, Plant, Cell & Environment, 18, 339–355, https://doi.org/10.1111/j.1365-3040.1995.tb00370.x, _eprint: https://onlinelibrary.wiley.com/doi/pdf/10.1111/j.1365-
425   3040.1995.tb00370.x, 1995.

Levenberg, K.: A method for the solution of certain non-linear problems in least squares, Quarterly of Applied Mathematics, 2, 164–168, https://doi.org/10.1090/qam/10666, 1944.

Lin, C., Gentine, P., Frankenberg, C., Zhou, S., Kennedy, D., and Li, X.: Evaluation and mechanism exploration of the diurnal hysteresis of ecosystem fluxes, Agricultural and Forest Meteorology, 278, 107 642, https://doi.org/10.1016/j.agrformet.2019.107642, 2019.

430 Liozon, R., Badeck, F.-W., Genty, B., Meyer, S., and Saugier, B.: Leaf photosynthetic characteristics of beech (Fagus sylvatica) saplings during three years of exposure to elevated CO(2) concentration, Tree Physiology, 20, 239–247, https://doi.org/10.1093/treephys/20.4.239, 2000.

Luo, X., Keenan, T. F., Chen, J. M., Croft, H., Colin Prentice, I., Smith, N. G., Walker, A. P., Wang, H., Wang, R., Xu, C., and Zhang, Y.: Global variation in the fraction of leaf nitrogen allocated to photosynthesis, Nature Communications, 12, 4866,

435 https://doi.org/10.1038/s41467-021-25163-9, number: 1 Publisher: Nature Publishing Group, 2021.

Marquardt, D. W.: An Algorithm for Least-Squares Estimation of Nonlinear Parameters, Journal of the Society for Industrial and Applied Mathematics, 11, 431–441, https://doi.org/10.1137/0111030, publisher: Society for Industrial and Applied Mathematics, 1963.

Martins, S. C. V., McAdam, S. A. M., Deans, R. M., DaMatta, F. M., and Brodribb, T. J.: Stomatal dynamics are limited by leaf hydraulics in ferns and conifers: results from simultaneous measurements of liquid and vapour fluxes in leaves, Plant, Cell & Environment, 39, 694–705,

440 https://doi.org/10.1111/pce.12668, _eprint: https://onlinelibrary.wiley.com/doi/pdf/10.1111/pce.12668, 2016.

Matthews, J. S., Vialet-Chabrand, S., and Lawson, T.: Acclimation to Fluctuating Light Impacts the Rapidity of Response and Diurnal Rhythm of Stomatal Conductance, Plant Physiology, 176, 1939–1951, https://doi.org/10.1104/pp.17.01809, 2018.

McAusland, L., Vialet-Chabrand, S., Davey, P., Baker, N. R., Brendel, O., and Lawson, T.: Effects of kinetics of light-induced stomatal responses on photosynthesis and water-use efficiency, New Phytologist, 211, 1209–1220, https://doi.org/10.1111/nph.14000, _eprint:

445 https://onlinelibrary.wiley.com/doi/pdf/10.1111/nph.14000, 2016.

Medlyn, B. E., Dreyer, E., Ellsworth, D., Forstreuter, M., Harley, P. C., Kirschbaum, M. U. F., Le Roux, X., Montpied, P., Strassemeyer, J., Walcroft, A., Wang, K., and Loustau, D.: Temperature response of parameters of a biochemically based model of photosynthesis. II. A review of experimental data, Plant, Cell & Environment, 25, 1167–1179, https://doi.org/10.1046/j.1365-3040.2002.00891.x, _eprint: https://onlinelibrary.wiley.com/doi/pdf/10.1046/j.1365-3040.2002.00891.x, 2002.

450 Medlyn, B. E., Duursma, R. A., Eamus, D., Ellsworth, D. S., Prentice, I. C., Barton, C. V. M., Crous, K. Y., De Angelis, P., Freeman, M., and Wingate, L.: Reconciling the optimal and empirical approaches to modelling stomatal conductance, Global Change Biology, 17, 2134–2144, https://doi.org/10.1111/j.1365-2486.2010.02375.x, _eprint: https://onlinelibrary.wiley.com/doi/pdf/10.1111/j.1365-2486.2010.02375.x, 2011.

Meeker, E. W., Magney, T. S., Bambach, N., Momayyezi, M., and McElrone, A. J.: Modification of a gas exchange sys-

455 tem to measure active and passive chlorophyll fluorescence simultaneously under field conditions, AoB PLANTS, 13, plaa066, https://doi.org/10.1093/aobpla/plaa066, 2021.

Miao, Z., Xu, M., Lathrop Jr., R. G., and Wang, Y.: Comparison of the A–Cc curve fitting methods in determining maximum ribulose 1·5-bisphosphate carboxylase/oxygenase carboxylation rate, potential light saturated electron transport rate and leaf dark respiration, Plant, Cell & Environment, 32, 109–122, https://doi.org/10.1111/j.1365-3040.2008.01900.x, _eprint:

460 https://onlinelibrary.wiley.com/doi/pdf/10.1111/j.1365-3040.2008.01900.x, 2009.

Miner, G. L., Bauerle, W. L., and Baldocchi, D. D.: Estimating the sensitivity of stomatal conductance to photosynthesis: a review, Plant, Cell & Environment, 40, 1214–1238, https://doi.org/10.1111/pce.12871, _eprint: https://onlinelibrary.wiley.com/doi/pdf/10.1111/pce.12871, 2017.

Naumburg, E. and Ellsworth, D. S.: Photosynthetic sunfleck utilization potential of understory saplings growing under elevated CO2 in FACE, Oecologia, 122, 163–174, https://doi.org/10.1007/PL00008844, 2000.

Noe, S. M. and Giersch, C.: A simple dynamic model of photosynthesis in oak leaves: coupling leaf conductance and photosynthetic carbon fixation by a variable intracellular CO2 pool, Functional plant biology: FPB, 31, 1195–1204, https://doi.org/10.1071/FP03251, 2004.

Oogathoo, S., Houle, D., Duchesne, L., and Kneeshaw, D.: Vapour pressure deficit and solar radiation are the major drivers of transpiration of balsam fir and black spruce tree species in humid boreal regions, even during a short-term drought, Agricultural and Forest Meteorology, 291, 108 063, https://doi.org/10.1016/j.agrformet.2020.108063, 2020.

Pearcy, R. W. and Seemann, J. R.: Photosynthetic Induction State of Leaves in a Soybean Canopy in Relation to Light Regulation of Ribulose-1-5-Bisphosphate Carboxylase and Stomatal Conductance 1, Plant Physiology, 94, 628–633, https://doi.org/10.1104/pp.94.2.628, 1990.

Rayment, M. B., Loustau, D., and Jarvis, P. G.: Measuring and modeling conductances of black spruce at three organizational scales: shoot, branch and canopy, Tree Physiology, 20, 713–723, https://doi.org/10.1093/treephys/20.11.713, 2000.

Rodgers, C. D.: Inverse Methods For Atmospheric Sounding: Theory And Practice, World Scientific, google-Books-ID: Xv7sCgAAQBAJ, 2000.

Sperry, J. S., Adler, F. R., Campbell, G. S., and Comstock, J. P.: Limitation of plant water use by rhizosphere and xylem conductance: results from a model, Plant, Cell & Environment, 21, 347–359, https://doi.org/10.1046/j.1365-3040.1998.00287.x, _eprint: https://onlinelibrary.wiley.com/doi/pdf/10.1046/j.1365-3040.1998.00287.x, 1998.

Sperry, J. S., Hacke, U. G., Oren, R., and Comstock, J. P.: Water deficits and hydraulic limits to leaf water supply, Plant, Cell & Environment, 25, 251–263, https://doi.org/10.1046/j.0016-8025.2001.00799.x, _eprint: https://onlinelibrary.wiley.com/doi/pdf/10.1046/j.0016-8025.2001.00799.x, 2002.

Sun, Y., Gu, L., and Dickinson, R. E.: A numerical issue in calculating the coupled carbon and water fluxes in a climate model, Journal of Geophysical Research: Atmospheres, 117, https://doi.org/10.1029/2012JD018059, number: D22 _eprint: https://onlinelibrary.wiley.com/doi/pdf/10.1029/2012JD018059, 2012.

Sun, Y., Gu, L., Dickinson, R. E., Norby, R. J., Pallardy, S. G., and Hoffman, F. M.: Impact of mesophyll diffusion on estimated global land CO2 fertilization, Proceedings of the National Academy of Sciences, 111, 15 774–15 779, https://doi.org/10.1073/pnas.1418075111, publisher: Proceedings of the National Academy of Sciences, 2014.

Venturas, M. D., Sperry, J. S., Love, D. M., Frehner, E. H., Allred, M. G., Wang, Y., and Anderegg, W. R. L.: A stomatal control model based on optimization of carbon gain versus hydraulic risk predicts aspen sapling responses to drought, New Phytologist, 220, 836–850, https://doi.org/10.1111/nph.15333, number: 3, 2018.

Vialet-Chabrand, S., Matthews, J. S. A., Brendel, O., Blatt, M. R., Wang, Y., Hills, A., Griffiths, H., Rogers, S., and Lawson, T.: Modelling water use efficiency in a dynamic environment: An example using Arabidopsis thaliana, Plant Science, 251, 65–74, https://doi.org/10.1016/j.plantsci.2016.06.016, 2016.

Vialet-Chabrand, S. R., Matthews, J. S., McAusland, L., Blatt, M. R., Griffiths, H., and Lawson, T.: Temporal Dynamics of Stomatal Behavior: Modeling and Implications for Photosynthesis and Water Use1[OPEN], Plant Physiology, 174, 603–613, https://doi.org/10.1104/pp.17.00125, number: 2, 2017.

Vialet-Chabrand, S., Dreyer, E., and Brendel, O.: Performance of a new dynamic model for predicting diurnal time courses of stomatal conductance at the leaf level, Plant, Cell & Environment, 36, 1529–1546, https://doi.org/https://doi.org/10.1111/pce.12086, number: 8 _eprint: https://onlinelibrary.wiley.com/doi/pdf/10.1111/pce.12086, 2013.

Wang, Y. and Frankenberg, C.: On the impact of canopy model complexity on simulated carbon, water, and solar-induced chlorophyll fluorescence fluxes, Biogeosciences, 19, 29–45, https://doi.org/10.5194/bg-19-29-2022, publisher: Copernicus GmbH, 2022.

Wang, Y., Sperry, J. S., Anderegg, W. R. L., Venturas, M. D., and Trugman, A. T.: A theoretical and empirical assessment of stomatal optimization modeling, New Phytologist, 227, 311–325, https://doi.org/10.1111/nph.16572, number: 2, 2020.

505 Wang, Y., Köhler, P., He, L., Doughty, R., Braghiere, R. K., Wood, J. D., and Frankenberg, C.: Testing stomatal models at the stand level in deciduous angiosperm and evergreen gymnosperm forests using CliMA Land (v0.1), Geoscientific Model Development, 14, 6741–6763, https://doi.org/10.5194/gmd-14-6741-2021, publisher: Copernicus GmbH, 2021.

Wang, Y., Köhler, P., Braghiere, R. K., Longo, M., Doughty, R., Bloom, A. A., and Frankenberg, C.: GriddingMachine, a database and software for Earth system modeling at global and regional scales, Scientific Data, 9, 258, https://doi.org/10.1038/s41597-022-01346-x,

510 number: 1 Publisher: Nature Publishing Group, 2022.

Wang, Y., Braghiere, R. K., Longo, M., Norton, A. J., Köhler, P., Doughty, R., Yin, Y., Bloom, A. A., and Frankenberg, C.: Modeling Global Vegetation Gross Primary Productivity, Transpiration and Hyperspectral Canopy Radiative Transfer Simultaneously Using a Next Generation Land Surface Model—CliMA Land, Journal of Advances in Modeling Earth Systems, 15, e2021MS002 964, https://doi.org/10.1029/2021MS002964, _eprint: https://onlinelibrary.wiley.com/doi/pdf/10.1029/2021MS002964, 2023.

515 Wolf, A., Anderegg, W. R. L., and Pacala, S. W.: Optimal stomatal behavior with competition for water and risk of hydraulic impairment, Proceedings of the National Academy of Sciences, 113, E7222–E7230, https://doi.org/10.1073/pnas.1615144113, publisher: Proceedings of the National Academy of Sciences, 2016.

Xu, L. and Baldocchi, D. D.: Seasonal trends in photosynthetic parameters and stomatal conductance of blue oak (Quercus douglasii) under prolonged summer drought and high temperature, Tree Physiology, 23, 865–877, https://doi.org/10.1093/treephys/23.13.865, number: 13,

520 2003.

Yuan, H., Dai, Y., Xiao, Z., Ji, D., and Shangguan, W.: Reprocessing the MODIS Leaf Area Index products for land surface and climate modelling, Remote Sensing of Environment, 115, 1171–1187, https://doi.org/10.1016/j.rse.2011.01.001, 2011.

Zeppel, M. J. B., Murray, B. R., Barton, C., and Eamus, D.: Seasonal responses of xylem sap velocity to VPD and solar radiation during drought in a stand of native trees in temperate Australia, Functional Plant Biology, 31, 461, https://doi.org/10.1071/FP03220, 2004.
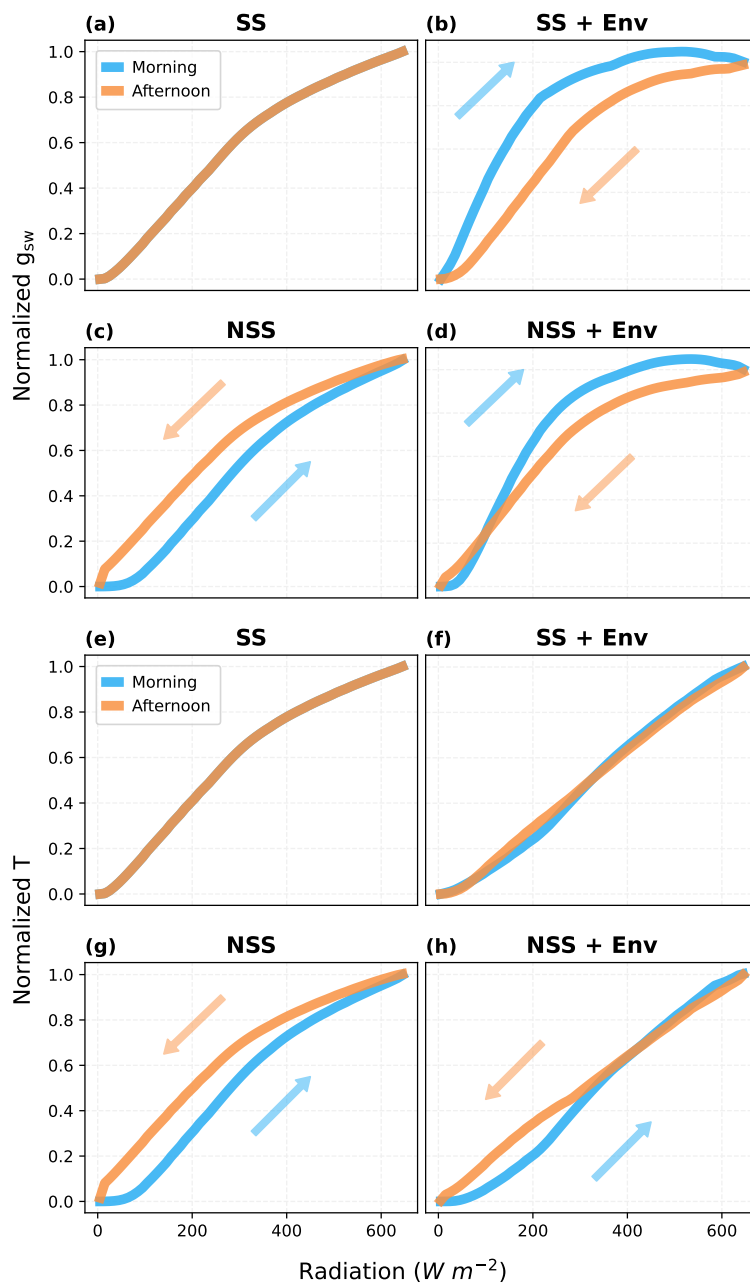
Figure 10. Hysteresis of the canopy-mean stomatal conductance (g_{sw}) and canopy transpiration rate (T) in response to radiation during an ideal clear-sky day. (a, e) SS model, (b, f) SS model with coupled diurnal variations of environmental conditions (Env, e.g. air temperature, VPD), (c, g) NSS model, (d, h) NSS model with Env. (a-d) normalized g_{sw} responses, (e-h) normalized T responses. In simulations without Env variations, except for the radiation, all the other environmental drivers were kept at the daytime means. g_{sw} and T is normalized with the values at noon (12:00). Arrows indicate the increasing and decreasing parts of the diurnal courses.
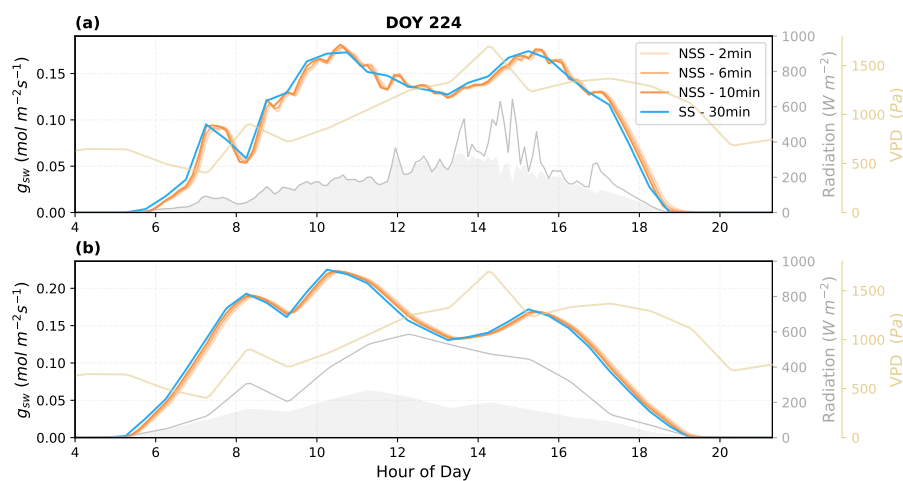
Figure 11. Simulations of dynamic g_{sw} using different time steps (2 min, 6 min, 10 min) and comparison with the traditional steady-state modeling (30-minute resolution) predictions. a) using high temporal-resolution PAR as radiation input, values are resampled accordingly to match the time step used; b) using ERA5 hourly radiation as input, values are linearly interpolated to 30-minute resolution. The shaded areas in gray under the radiation curves represent the diffuse component of the total radiation.